

RESEARCH ARTICLE | NOVEMBER 14 2023

Exciton–polaron interactions in metal halide perovskite nanocrystals revealed via two-dimensional electronic spectroscopy

Special Collection: [Festschrift in honor of Louis E. Brus](#)

Patrick Brosseau ; Arnab Ghosh ; Helene Seiler ; Dallas Strandell ; Patanjali Kambhampati  

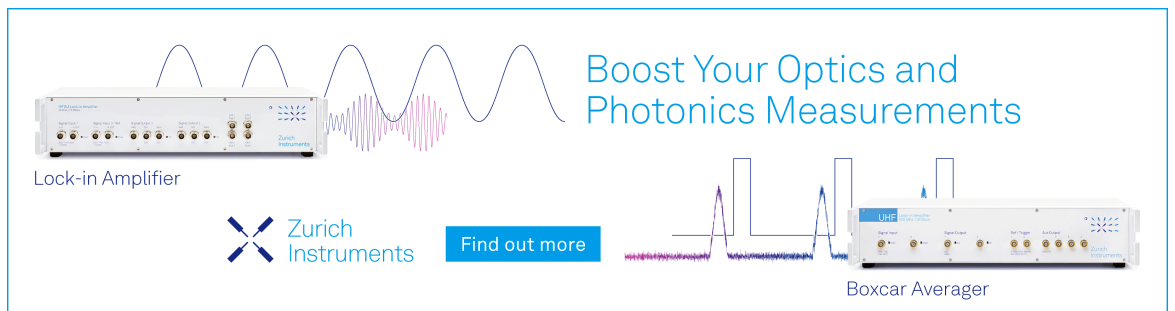


J. Chem. Phys. 159, 184711 (2023)

<https://doi.org/10.1063/5.0173369>



CrossMark



Boost Your Optics and Photonics Measurements

Lock-in Amplifier

Zurich Instruments

Find out more

Boxcar Averager

Exciton–polaron interactions in metal halide perovskite nanocrystals revealed via two-dimensional electronic spectroscopy

Cite as: J. Chem. Phys. 159, 184711 (2023); doi: 10.1063/5.0173369

Submitted: 21 August 2023 • Accepted: 19 October 2023 •

Published Online: 14 November 2023



View Online



Export Citation



CrossMark

Patrick Brosseau,^{a)} Arnab Ghosh,^{b)} Helene Seiler,^{b)} Dallas Strandell,^{a)} and Patanjali Kambhampati^{a)}

AFFILIATIONS

Department of Chemistry, McGill University, Montreal, Quebec H3A 0B8, Canada

Note: This paper is part of the JCP Festschrift in honor of Louis E. Brus.

^{a)} Author to whom correspondence should be addressed: pat.kambhampati@mcgill.ca

^{b)} Present address: Freie Universität Berlin, Physics Department, Arnimallee 14, 14195 Berlin, Germany

ABSTRACT

Metal halide perovskite nanocrystals have been under intense investigation for their promise in optoelectronic devices due to their remarkable physics, such as liquid/solid duality. This liquid/solid duality may give rise to their defect tolerance and other such useful properties. This duality means that the electronic states are fluctuating in time, on a distribution of timescales from femtoseconds to picoseconds. Hence, these lattice induced energy fluctuations that are connected to polaron formation are also connected to exciton formation and dynamics. We observe these correlations and dynamics in metal halide perovskite nanocrystals of CsPbI₃ and CsPbBr₃ using two-dimensional electronic (2DE) spectroscopy, with its unique ability to resolve dynamics in heterogeneously broadened systems. The 2DE spectra immediately reveal a previously unobserved excitonic splitting in these 15 nm NCs that may have a coarse excitonic structure. 2D lineshape dynamics reveal a glassy response on the 300 fs timescale due to polaron formation. The lighter Br system shows larger amplitude and faster timescale fluctuations that give rise to dynamic line broadening. The 2DE signals enable 1D transient absorption analysis of exciton cooling dynamics. Exciton cooling within this doublet is shown to take place on a slower timescale than within the excitonic continuum. The energy dissipation rates are the same for the I and Br systems for incoherent exciton cooling but are very different for the coherent dynamics that give rise to line broadening. Exciton cooling is shown to take place on the same timescale as polaron formation, revealing both as coupled many-body excitation.

Published under an exclusive license by AIP Publishing. <https://doi.org/10.1063/5.0173369>

I. INTRODUCTION

Metal-halide perovskites (MHPs) have been under intense investigation for their performance in photovoltaics initially, rapidly surpassing the performance of other materials, including semiconductor quantum dot (QD) based photovoltaics.^{1,2} In this application, the key observation was high efficiency and good transport properties despite highly defective materials, in contrast to the search for perfection that is the case in standard covalent semiconductors from Si to CdSe. Following the initial work on MHPs, nanocrystal (NC) versions have become available as MHP NCs.³ In the case of MHP NCs, they have found tremendous promise in light emissive applications, such as lasers and light emitting diodes (LEDs), in addition to light absorptive applications found for thin films.^{4,5} MHP NCs are known for their high photoluminescence (PL) quantum yields,³ fast

radiative emission,⁶ and long coherence times for sources of single and entangled photons⁷ and superfluorescence.⁸

A key feature of these perovskites is their defect tolerance.⁹ This defect tolerance is thought to arise from the details of the lattice, which is ionic and characterized by strongly anharmonic bonds, lacking a well-resolved vibrational spectrum at room temperature.^{10,11} It is particularly the vibrational spectra and the dielectric dispersion spectra^{12–14} that give rise to a picture of LHPs in which they are phonon glass/electron crystals (PGECs) by virtue of their liquid–solid duality.^{15,16} The phonon space behaves as a glass, whereas the electron space behaves as a crystal, with band-like transport, as discussed by Zhu.^{17–22} Since the lattice structural dynamics are glassy, as also revealed by ultrafast diffraction experiments,^{23,24} the important lattice modes are localized and diffusively moving polarons rather than delocalized and coherently moving phonons.

The polarons that characterize LHPs are central to their unique and favorable optical properties.

In the case of NCs of LHPs and two-dimensional materials, e.g., Ruddelston–Popper type perovskites, the presence of excitons is also important. In the case of QDs of LHPs, one sees excitonic transitions consistent with strongly confined CdSe QDs.^{25,26} In the case of the more common weakly confined (twice the Bohr length) NCs, there are still fast radiative rate constants⁶ and fine structure splittings^{27–29} consistent with excitonic behavior. Moreover, larger QDs or NCs may have hidden splittings within the heterogeneous broadening of the sample. In the case of two-dimensional materials,^{11,30,31} these effects are even stronger with larger 200 meV excitonic binding energies due to reduced screening. In covalent semiconductors, one has exciton–phonon coupling to measure the degree of interaction. In contrast, these ionic and anharmonic LHPs have exciton–polaron coupling, which is to be assessed in terms of its importance to the functioning of the material.

A number of femtosecond laser spectroscopic experiments have been performed on MHPs in order to identify the polaron and also to identify hot carrier cooling dynamics toward the band edge exciton at high excess energy.^{11,19–21,24,30,32–42} These studies have suggested that the polarons form on the sub-ps timescale and couple to excitons. Hot carrier relaxation is shown to take place on a distribution of timescales, based upon the excess electronic energy within the system. Recently, we have shown⁴⁴ via two-dimensional electronic (2DE) spectroscopy that the electronic lineshapes of CsPbI₃ P NCs follow diffusive lattice structural dynamics consistent with a glassy or liquid state and inconsistent with covalent semiconductors, which undergo ballistic structural dynamics via coherent phonons. Following the direct observation of polaron formation in LHP NCs, we then used one-dimensional transient absorption (TA) spectroscopy⁴² to indirectly suggest the coupling of polarons to excitons. The TA data on CsPbBr₃ P NCs revealed that the formation of polarons resulted in further quantum confinement effects upon the excitons, for the weakly confined (15 nm) NCs probed. In short, there is a growing body of evidence of exciton–polaron coupling in a manner similar to electron solvation in solids rather than in liquids.¹⁶

What is needed is a direct measure of the impact of exciton–polaron interactions in model systems of 15 nm LHP NCs that are the model P NC system since their inception in 2015 by Kovalenko *et al.*³ These model systems are the most studied in terms of their single dot PL spectra of fine structure and their ultrafast spectroscopy of dynamics. Here, we perform 2DE spectroscopy on the model system of weakly confined 15 nm MHP NCs of CsPbI₃ and CsPbBr₃ P NCs to specifically unravel these interactions. 2DE spectroscopy is uniquely powerful as an ultrafast spectroscopic method in that not only can new dynamics be obtained,^{45,46} but they can also be obtained in the presence of heterogeneous broadening.⁴⁷ Moreover, 2DE has an unprecedented combination of time and energy resolution that is not possible in 1D TA spectroscopy. The 2DE spectra immediately reveal a previously unobserved electronic splitting that was not visible in 1D spectroscopies.^{41,42} The peak splitting shows dynamics on the 10 fs timescale, illustrating the extreme efficiency of excitonic cooling in this regime close to the band edge exciton. The 2DE spectra enable observation of 2D lineshape dynamics, which are shown to reveal liquid-like responses due to polaron formation in both systems on the 300 fs timescale. The impact of the polaron dynamics upon the TA spectra is a dynamic

broadening and blueshifting due to exciton–polaron interactions. The excited states relax on the same 300 fs timescale as polaron formation, illustrating that the coupling is dynamic.

II. EXPERIMENT

2DES experiments were conducted on a previously described instrument^{44,46–52} using nonclassical optics of hollow core fibers and acousto-optic modulators. The 2DES measurements of CsPbI₃ were conducted using the output of a Ti:sapphire amplifier (Coherent Legend Elite Duo HE+, 800 nm, 1 kHz, 130 fs) spectrally broadened in a hollow core fiber (two-cycle, length = 2.5 m, inner diameter = 400 μm) filled with 3 atm of argon in a pressure gradient. The 2DES measurements of CsPbBr₃ were conducted using the output of a commercial optical parametric amplifier (Light Conversion, Topas), centered at 500 nm and spectrally broadened in a hollow core fiber filled with 3 atm of argon. In both cases, the output of the hollow core fiber is temporally stretched in a grism pair before being split between two acousto-optic pulse shapers (Fastlite, Dazzler). The pulse shapers compress the pulses to 18–20 fs, as confirmed by transient-grating frequency resolved optical gating (TG-FROG), as shown in Fig. S1.

One of the pulse shapers diffracts two pulses, separated by a time delay t_1 and phase difference ϕ , to be used as a pump beam. The other pulse shaper diffracts a single pulse to act as the probe. The pump beam crosses the sample at an angle and is stopped by a beam block, while the probe is transmitted straight through the sample and into a CCD spectrometer (Acton 2500i, PIXIS 100B Excelon). To measure a single 2DES spectrum, the time delay between the pump and probe pulses, t_2 , is kept constant, while the time delay between the two pump pulses, t_1 , is varied. A $2 \times 2 \times 1$ phase cycling scheme is used where the phase of the first two pulses is set to $\phi = 0$ and $\phi = \pi$ for each value of t_1 . A rotating frame is applied to the second pulse relative to the first pulse. The data are Fourier transformed along t_1 to generate a two-dimensional (E_1, E_3) map.

III. BACKGROUND ON PEROVSKITES AND 2D SPECTROSCOPY

Figure 1 provides an overview of the idea of structural dynamics in MHP NCs. Figure 1(a) shows the linear absorption and the photoluminescence (PL) spectra along with the laser spectra for the CsPbBr₃ and CsPbI₃ LHP NCs. The laser spectra are tuned to probe near the band edge and the PL. Figure 1(b) shows a schematic illustration of the perovskite lattice as a cubic NC, as are these. The length of the NC is 15 nm, and shown is a 7 nm polaronic distortion of the lattice. Also shown is an exciton confined to the polaronic region of 7 nm length.

Figure 1(c) schematically illustrates the relevant processes involved in the structural dynamics at the level of excitons and the lattice. Due to strong electron–phonon interactions, a configuration coordinate diagram must be considered rather than a purely electronic level diagram. Due to the glassy and anharmonic nature of the MHP lattice, the phonon coordinate is less important than the polaron coordinate. This idea of low frequency continuum modes is revealed in the Raman spectra and their temperature dependence.^{10,11,16,53} One does not see discrete phonons at

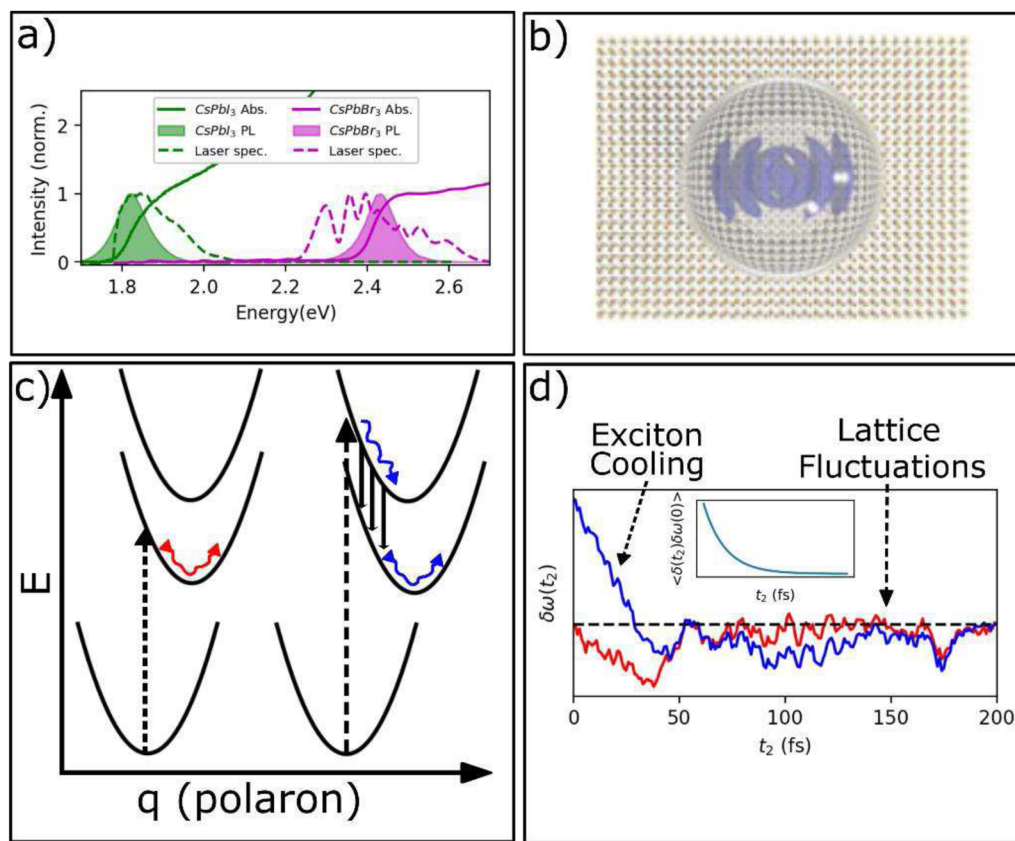


FIG. 1. Overview of the structure of lead halide perovskite nanocrystals (LHP NCs) and their spectroscopy in terms of exciton–polaron interaction. (a) Linear absorption spectra, photoluminescence (PL) spectra, and laser spectra for the 15 nm NCs of CsPbI₃ and CsPbBr₃ LHPs. (b) Schematic illustration of a perovskite lattice undergoing a polaronic distortion, giving rise to a potential well of 7 nm length. In the NCs are excitons with Bohr lengths of 7 nm, half the diameter. (c) Illustration of lattice structural dynamics during polaron formation (left, red) and exciton cooling and polaron formation (right, blue). (d) The energy gaps in LHPs are stochastic due to their glassy nature (red). Cooling proceeds on the same timescale as the correlation function describing the fluctuations.

room temperature; instead, there is a spectral density that represents the polaron spectrum. Upon excitation, polaron formation will spontaneously proceed in a dissipative and diffusive manner,⁴⁴ as reflected by the arrow. Since the band edge state is excitonic, it is exciton–polaron coupling that is the key idea. If there is a higher energy state, excitonic or continuum, relaxation will take place. Illustrated is a higher energy excitonic state, from which hot exciton cooling will take place. The cooling process may take place on the same timescale as polaron formation, also reflecting exciton–polaron coupling.

These processes of cooling vs fluctuations are schematically illustrated in Fig. 1(d). Shown is the mean energy of a single particle's trajectory, either from an excited state or about equilibrium, such as the cooled band edge exciton. The hot exciton will undergo energy relaxation in a fluctuating manner. In addition, it may take place on the same timescale as the correlation function that describes the equilibrium fluctuations, as shown in the inset.

To better understand the nature of the 2DE spectra and how they reveal unique information,^{54–58} see Fig. 2, which schematically identifies the signals and processes via model simulations.

Figure 1(a) shows the standard problem of NC spectroscopy of heterogeneous broadening. Of course, single particle spectroscopy is a useful method to bypass this form of broadening. However, it only yields PL spectra and the slowest of kinetic processes. Hence, one needs absorptive spectroscopies done at the ensemble level to probe the earliest processes that take place on the fs and ps timescales. Shown is a Gaussian distribution of single NC spectra that are Lorentzian, giving rise to a Voigt lineshape for absorption, or PL. In 1D spectroscopies, such as TA, there remains heterogeneous broadening in the signals. In contrast, 2DE enables overcoming heterogeneous broadening.

Figure 2(b) schematically illustrates a 2DE spectrum and the information contained within it. We define E_1 as the excitation axis and E_3 as the detection axis. See the supplementary material for a fuller discussion of the theory and methods of 2DE. Enabled by Fourier methods, one has a 2D spectrum. The main idea is to look for peaks along the energy diagonal and the energy off-diagonal. Provided one measures 2DE spectra as a function of time, t_2 , or population time, one now has a series of time dependent 2DE spectra with which to assess lineshape dynamics. The first peak along the

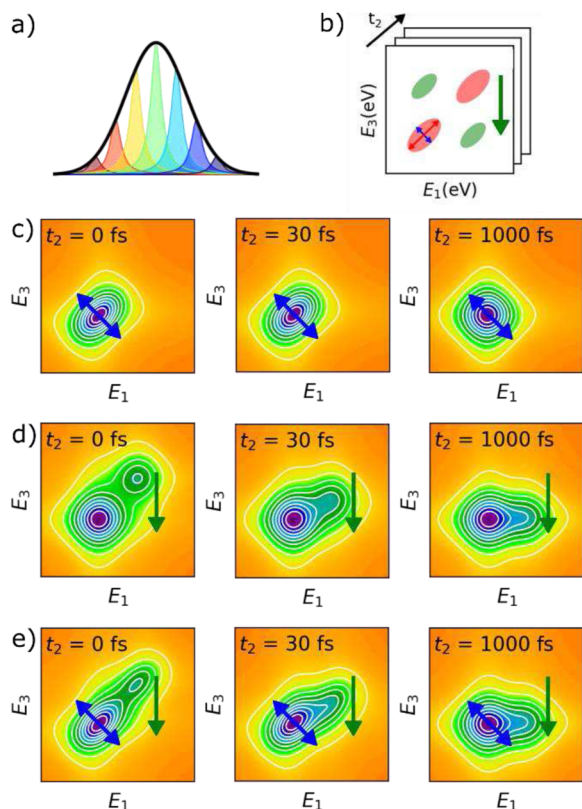


FIG. 2. Overview of how two-dimensional electronic (2DE) spectroscopy reveals information even in the presence of heterogeneous broadening. (a) A single NC will have a Lorentzian spectrum with a Gaussian spectral distribution, giving rise to a Voigt spectrum for the heterogeneously broadened ensemble spectrum in 1D. (b) Schematic illustration of the information contained in 2DES. There are diagonals and off-diagonals, with positions and 2D linewidths, which are discussed in the text. (c) Schematic illustration of spectral diffusion following a Kubo lineshape. The key observable is the anti-diagonal linewidth. (d) Schematic illustration of hot exciton relaxation on a 100 fs timescale. (e) Schematic illustration of the presence of both spectral diffusion and energy relaxation.

diagonal corresponds to the lowest energy state, or the band edge exciton. Any higher lying peaks would be seen at higher energy along the diagonal. Along the off-diagonal, one might see signals that arise due to coupling between excitonic states. These couplings are usually independent. In contrast, there will be dynamics in the upper diagonal peak as it relaxes toward equilibrium. For the peaks along the diagonal, one can further analyze their 2D lineshapes, which reflect homogeneous and inhomogeneous broadening.

Figures 2(c)–2(e) illustrate by simulation the basic processes in lineshape dynamics, cooling dynamics, and the presence of both as a coupled process. Shown are the 2DE spectra at population times, t_2 , of 0, 30, and 1000 fs. The lineshape dynamics in Fig. 2(c) are assumed to follow a Kubo functional form. The cooling dynamics in Fig. 2(d) are assumed to follow an exponential functional form. In addition, the mixture of the coupled system is shown in Fig. 2(e).

IV. RESULTS AND DISCUSSION

Experimental 2DE data for both MHP NCs are shown in Fig. 3. Shown are the 2DE spectra at a population time of $t_2 = 0, 100,$ and 1000 fs. Also shown for comparison are the linear absorption spectra. The immediate observation from the 2DE spectra, in contrast to the linear spectra and 1D TA spectra,^{41,42} is the presence of a doublet of peaks. The peak splitting is 120 and 70 for CsPbI₃ and CsPbBr₃, respectively, as measured at $t_2 = 1000$ fs. Table I presents a summary of the values for all the time constants and amplitudes of the energetic processes. These two peaks are inhomogeneously broadened by 50 meV compared to the linear absorption spectra. The absorption spectra are featureless and do not resolve this hidden peak. This doublet could arise from quantum size effects, which yield a spectrum of states as shown in NCs smaller than 10 nm.²⁵ In these smaller NCs, the 1S–1P splitting can be 100–200 meV. However, these are 15 nm NCs, which are twice the Bohr length; hence, they are weakly confined or bulk-like. As such, the linear absorption spectra show no doublet for this size. However, the linear absorption spectra are inhomogeneously broadened, which is bypassed by the resolving ability of the 2DE spectra. In addition, all other experiments, whether linear absorption or transient absorption, on these model system 15 nm NCs are consistent in that there is no doublet observed.¹⁵ These 2DE experiments, with their unique spectroscopic capacity, are the first to reveal this previously unobserved excitonic structure. Future size dependent experiments are underway to better understand the nature of this peak splitting into a doublet.

Above the diagonal, there are positive photoinduced state absorption (PIA) signals that may arise from either biexciton formation^{47,59} or from excitation induced activation of forbidden transitions.⁶⁰ They will not be further discussed, as more emphasis will be placed on the negative signals below the diagonal. The total signal is comprised of contributions from ground state bleaching (GSB), stimulated emission (SE), and excited state absorption (ESA) components, as commonly discussed in nonlinear spectroscopy. These three terms result in PIA or negative signals. The diagonal corresponds to the same excitation and detection energies. In contrast, given some initial excitation energy (E_1) and some lower detection energy (E_3), one can monitor energy relaxation from the upper to the lower state. This process will be discussed in further detail below. Along the diagonal, especially for the lower energy band edge excitation, one sees lineshape dynamics that will be discussed in detail below.

To focus on energy relaxation dynamics, close to the band edge, Fig. 4 presents the trajectories of the 2DE signals along the four main integration areas. Shown are the 2DE spectra of both NCs, along with areas of integration corresponding to diagonals and off-diagonals as discussed above. The four transients each reflect complex dynamics due to signals arising from different processes of coupling, bleaching, and relaxation. The two transients of most importance to probing hot exciton relaxation dynamics are shown in the figure in yellow ($E_1 = E_3$) and red ($E_1 > E_3$). The transients in yellow show an instrument response function (IRF) limited rise in the bleach, followed by a slight decay. In contrast, the transients in the red show a slow buildup. As we have discussed in detail for exciton cooling dynamics in CdSe QDs, these signals can be subtracted to produce a $\Delta\Delta$ OD signal, which directly monitors the population dynamics.^{61–65} This double differential signal is shown here for both

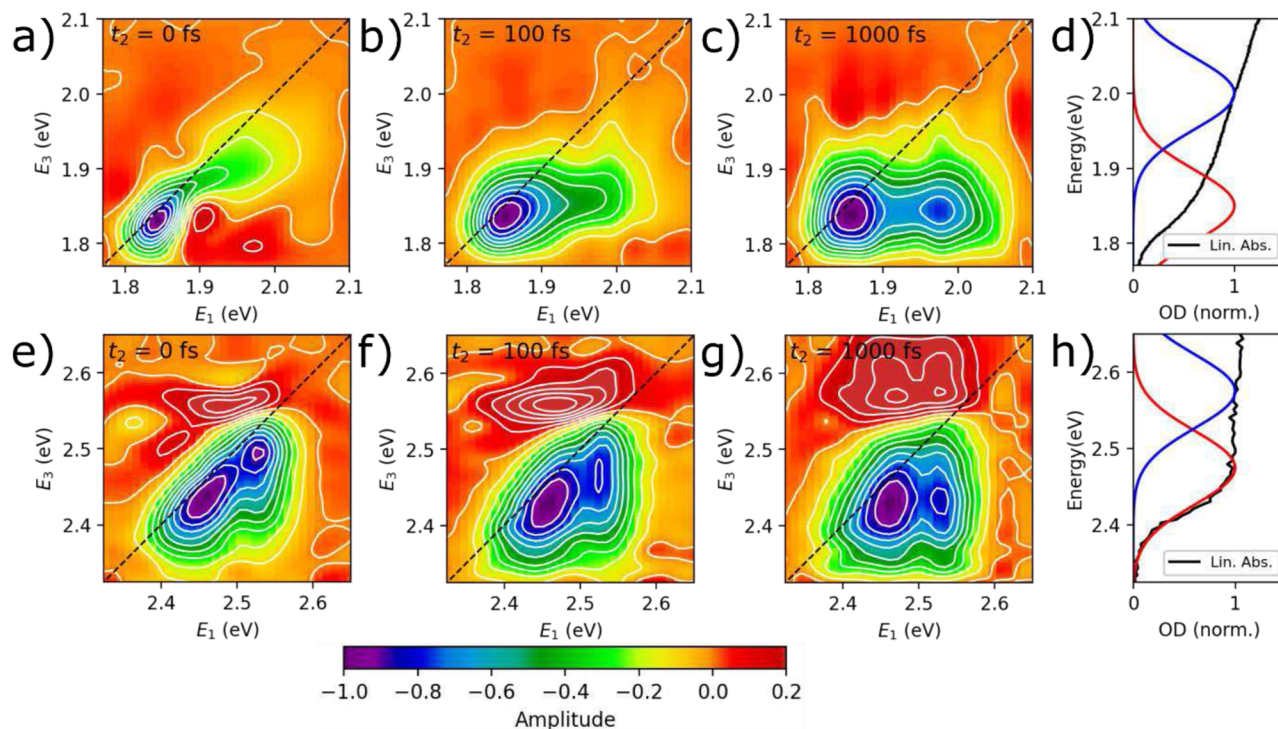


FIG. 3. 2DE spectra and linear absorption spectra of CsPbI₃ [(a)–(d)] and CsPbBr₃ LHP NCs [(e)–(h)]. 2DE spectra are shown at population times (t_2) of 0, 100, and 1000 fs. The linear absorption spectra show the doublet broadened heterogeneously. The 2DE spectra reveal two distinct features, with peak splittings of 120 and 70 meV, respectively, for CsPbI₃ and CsPbBr₃, measured at $t_2 = 1000$ fs.

samples and is shown to decay with time constants of 215 and 194 fs, respectively. These time constants correspond to relaxation rates of 0.65 and 0.62 eV/ps, respectively, showing a similar timescale for hot carrier cooling in both samples. The $\Delta\Delta\text{OD}$ can be alternatively

defined to more closely match our 1D state-resolved pump/probe (SRPP) experiments^{41,42,61,62,64,65} by subtraction of the red from the blue integration areas. Doing so yields slightly different relaxation rates but with values that remain similar across materials, as noted

TABLE I. Parameters from the 2DE spectra.

	CsPbI ₃	CsPbBr ₃	Ratio I/Br
Atomic mass (amu)	126.9	79.9	R = 1.59 $\sqrt{R} = 1.26$ $R^2 = 2.53$
2DE peak splitting (meV)	120	70	1.71
2DE cooling time (fs)	215	194	1.11
2DE energy cooling rate (eV/ps)	0.65	0.62	1.05
Pseudo-TA peak shift amplitude (meV) for red excitation	7.5	10	0.75
Pseudo-TA peak shift timescale (fs) for red excitation	241	1092	0.22
Pseudo-TA peak shift rate (eV/ps) for red excitation	0.03	0.01	3.00
Pseudo-TA peak shift amplitude (meV) for blue excitation	-25	-16	1.56
Pseudo-TA peak shift timescale (fs) for blue excitation	701	241	2.91
Pseudo-TA peak shift rate (eV/ps) for blue excitation	0.04	0.07	0.57
Spectral diffusion amplitude (meV)	41	60	0.68
Spectral diffusion timescale (fs)	375	300	1.25
Spectral diffusion rate (eV/ps)	0.11	0.20	0.55

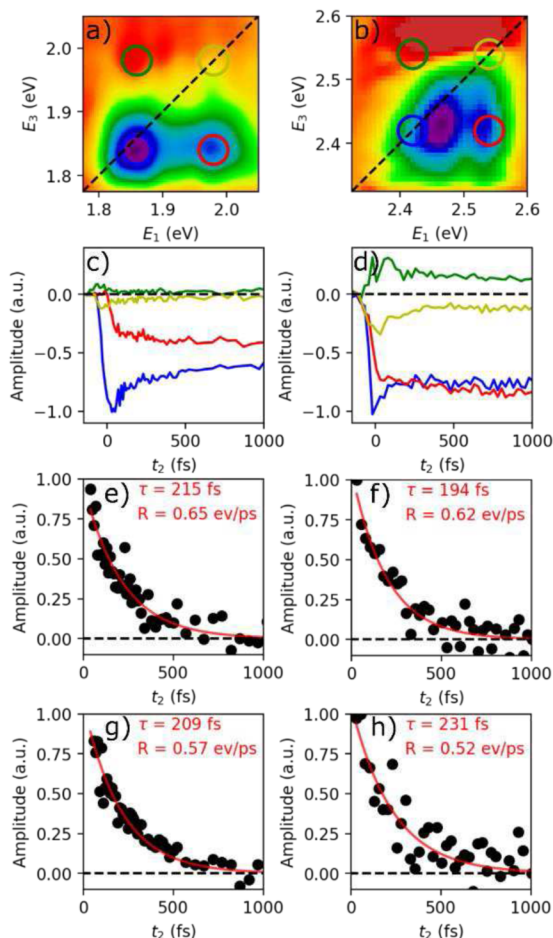


FIG. 4. Obtaining hot exciton cooling dynamics from 2DE spectra. (a) 2DE spectrum at $t_2 = 1000$ fs, along with four areas of spectral integration to obtain transients for CsPbI₃ LHP NCs. (b) 2DE spectrum at $t_2 = 0$ fs, along with four areas of spectral integration to obtain transients for CsPbBr₃ LHP NCs. (c) and (d) The resulting spectral transients. (e) and (f) The $\Delta\Delta\text{OD}$ signal reflecting the excited state population decay, subtracting the red from the yellow transients. (g) and (h) The $\Delta\Delta\text{OD}$ signal reflecting the excited state population decay, subtracting the red from the blue transients.

in Table I. As we have discussed in detail elsewhere,^{62–69} SRPP is a variation of a TA experiment in which two resonant pump colors are chosen and alternated in real time. This real time alternation of pump colors enables careful comparison and subtraction of TA spectral transients obtained under these two pumping conditions.

Having detected a previously unobserved excitonic splitting, followed by ultrafast hot exciton relaxation, the question arises of competing and coupled processes of line broadening due to polaron formation and line shifting due to cooling. As shown in Fig. 2 and in the supplementary material, the 2DE spectra can be decomposed to reveal lineshape dynamics. Importantly, there are different lineshapes that can be measured. One has the 2D lineshape, in which there is a diagonal and an anti-diagonal width. These widths are well discussed in the 2D literature^{44,50,54–57,70,71} and the supplementary material. The diagonal represents the total linewidth,

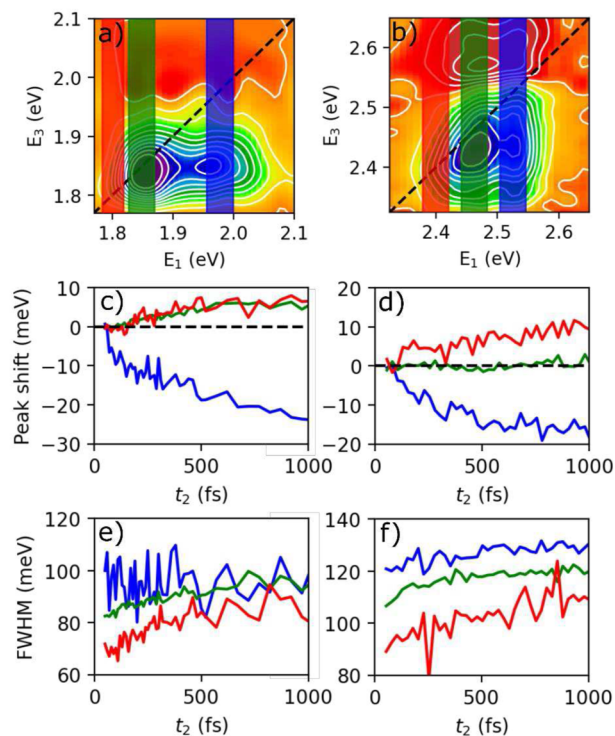


FIG. 5. Spectral lineshape analysis in both 2DE and 1D TA forms. Anti-diagonal 2DE linewidth trajectories for CsPbI₃ and CsPbBr₃ LHP NCs, (a) and (b), respectively. The 2DE spectra can produce TA spectra with band edge bleaching signals that yield trajectories for linewidth (c) and peak shift (d) for CsPbI₃. [(e) and (f)] *ibid* for CsPbBr₃ LHP NCs. See Table I for the numbers obtained from these data.

and the anti-diagonal represents the homogeneous linewidth, evolving in time. The 2DE spectra can also be projected into pseudo-TA spectra (shown in the supplementary material), which reveal optical bleaching linewidths that are distinct from the homogeneous and inhomogeneous linewidths in the 2DE data.

We begin the exploration of lineshape dynamics by focusing on the 1D pseudo-TA spectra that one can obtain by spectrally integrating along the excitation energy, E_1 , for some bandwidth. Figures 5(a) and 5(b) shows the 2DE spectra with integration windows in the red (to the red of the X1 peak), in the green (on the X1 peak), and in the blue (on the X2 peak). The supplementary material shows the raw data for the pseudo-TA spectra, or equivalently, the SRPP spectra. These spectra are analyzed by fitting the featureless bleach spectrum to a Gaussian of some width and peak energy. These data then enable peak width and peak center trajectories to be shown in Figs. 5(c)–5(f). By virtue of the unique energy/time resolution of 2DE that is not possible in 1D TA, the pseudo-TA spectra can be obtained at selected excitation energies, E_1 . The spectral selection of the three excitation energies is shown in the supplementary material. These spectral selections are useful in different ways. The spectral selection in red minimizes inhomogeneous broadening by selecting the reddest NC in the ensemble. The spectral selection in the blue reflects hot exciton cooling. The spectral selection in green is less useful than the other two.

The most striking behavior is the optical bleach blueshifting and broadening on the 300 fs timescale for the red excitation. We have previously observed this phenomenon in TA experiments of CsPbBr₃ LHP NCs and had assigned the spectral dynamics to exciton–polaron coupling.⁴² We proposed that as the polaron forms, a potential well is created, which dresses the exciton as it was originally formed in the 15 nm NCs. The exciton is now coupled to this 7 nm lattice distortion in the polaron. This confinement effect can either lower (redshift) or raise (blueshift) the total transition energy as per a number of interactions between excitons and the lattice, which are only now being discussed. We hope that these results stimulate theory to be able to precisely rationalize the observed phenomena. We had discussed this idea of exciton–polaron coupling in light of electron solvation in the solid state,^{16,42} as have Silva,^{11,30,31} Zhu,^{17–20,22} and Brus.^{10,72}

Excitation into the upper exciton (blue) reveals linewidth and energy trajectories that reflect hot exciton cooling and polaron formation taking place in parallel. These numbers coincide with the numbers obtained in the 2DE subtraction analysis and robustly reflect hot exciton cooling, which is taking place in parallel with polaron formation. Table I shows the values of the hot exciton cooling rates in eV/ps for the different spectroscopic methods, each revealing a similarity across samples for this incoherent process of hot exciton cooling.

The energy dissipation rate is 0.6 eV/ps at this energy using the simplest version of 2DE to go beyond 1D-TA experiments. In order to more fully exploit the energy/time capabilities of 2DE, we perform a more detailed analysis of energy relaxation in Fig. 6. Figures 6(a) and 6(b) show the 2DE spectra of both NCs at a population time $t_2 = 1000$ fs. Shown on each spectrum are integration areas, along the energy diagonal, corresponding to having linear excess energy, and the energy horizontal, corresponding to zero excess energy. From these integration areas the timescale and the energy dissipation rate (eV/ps) can be obtained as a function of excess energy. Figures 6(c) and 6(d) show the data for both NCs. There are several common features. The relaxation rate is zero near zero excess energy. The relaxation rate increases with energy over this initial regime to 0.6 eV/ps, with regions of differing slopes. The discontinuities in slope are marked by a peak in the dissipation rate that coincides with the excitonic peaks, X1 and X2.

These 2DE spectra illustrate the exciton cooling dynamics for the lowest energy states of MHP NCs. How do these rates connect to the energy dissipation rates for excitation into the continuum at 3.1 eV? The overall value for excitation at 3.1 eV as evaluated by generic 1D TA measurements is 3.0 eV/ps.^{73–80} When excited into the continuum at 3.1 eV, the relaxation dynamics follow a cascade of processes taking place on a longer timescale.^{41,42} We have previously shown a breaking of the phonon bottleneck in MHP NCs via Auger processes.^{41,42} These Auger processes, moreover, are dynamic due to the competing polaron formation. This competition results in a time dependent rate constant for hot exciton cooling.⁴² A time dependent rate constant illustrates a transition from population kinetics, regardless of timescale, to quantum dynamics that obey non-exponential time dependence.⁸⁰ From our SRPP work, we showed that this initial cooling rate of 3 eV/ps actually begins at a higher value of 5 eV/ps and then slows down closer to the band edge after 300 fs to a value of 0.6 eV/ps. Figure 6(e) shows the carrier cooling rates as evaluated by SRPP and 2DE. In the case of SRPP,

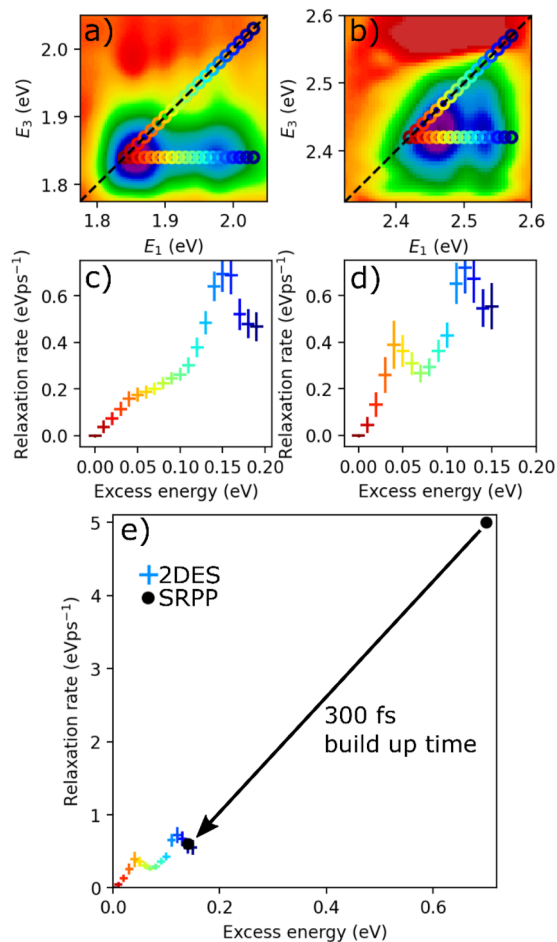


FIG. 6. High resolution hot exciton cooling dynamics. (a) CsPbI₃ 2DE spectrum. (b) CsPbBr₃ 2DE spectrum. (c) CsPbI₃ relaxation rate as a function of excess energy, measured by fitting the off-diagonal transient from the on-diagonal transient for every value of excess energy. (d) CsPbBr₃ relaxation rate as a function of excess energy, measured by fitting the off-diagonal transient from the on-diagonal transient for every value of excess energy. (e) CsPbBr₃ relaxation rate as a function of excess energy with values measured by state-resolved pump–probe (SRPP).

there are only two energy points, and it is assumed there is a linear interpolation between these two limits in the absence of any other observation. Remarkably, the low energy long time value of 0.6 eV/ps from SRPP is identical to the value obtained by 2DE, at its highest energy currently possible to probe. With increases in light source bandwidth in the blue, we aim to be able to more fully resolve these dynamics in future experiments.

Thus far, we have focused on the lineshape dynamics of the equivalent 1D TA or SRPP spectra. In addition, the dynamics that were observed were the incoherent dynamics of population relaxation through a manifold of excitonic states with strong vibronic/polaronic dressing. As noted above, 2DE spectroscopy can also report unique 2D information, such as diagonal and anti-diagonal lineshape dynamics. Figures 7(a) and 7(b)

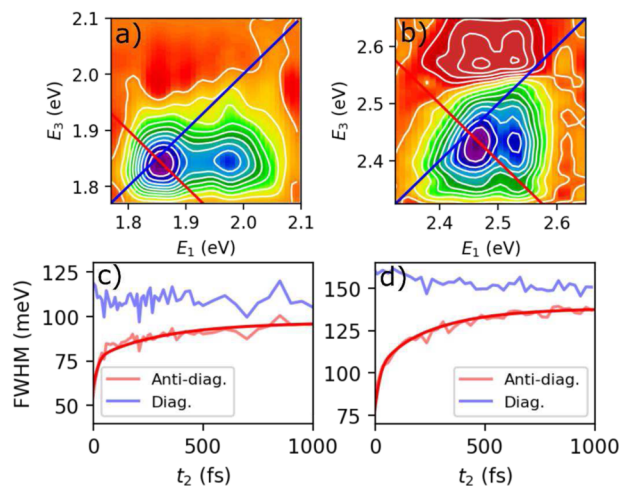


FIG. 7. Monitoring spectral diffusion in the band edge state. The blue and red lines show the diagonal and anti-diagonal slices through the 2DES spectra at $t_2 = 1000$ fs for (a) CsPbI₃ and (b) CsPbBr₃. The FWHM of the diagonal (blue) narrows, while the anti-diagonal (red) broadens. Modeling the anti-diagonal (solid red line) gives a spectral diffusion timescale of $\tau = 375$ fs for CsPbI₃ and $\tau = 300$ fs for CsPbBr₃, giving a ratio of 1.25. The square root of the mass ratio for the anions is 1.26.

show the linewidth dynamics for both MHP NCs. We have previously reported on the lineshape dynamics of CsPbI₃ MHP NCs,⁴⁴ and new data are shown for the more common and more stable CsPbBr₃ system. The anti-diagonal linewidth broadens on 375 and 300 fs timescales for CsPbI₃ and CsPbBr₃ P NCs, respectively. Table I shows the details of the timescales, amplitudes, and energy dissipation rates.

We propose this spectral diffusion to arise from lattice fluctuations propagating motion in an incoherent and diffusive manner towards the polaronic minimum along this collective coordinate. We model the frequency–frequency correlation function (FFCF) for spectral diffusion phenomenologically with a Kubo lineshape, assuming that the FFCF is purely dissipative and non-oscillatory. Further details are given in our prior work⁴⁴ and in the supplementary material. The amplitude and timescale of the fluctuations are strongly dependent upon the cation, as is especially shown by the energy fluctuation rate (eV/ps) being twice as large for the Br system. These 2DE lineshape measurements reveal complex lineshape dynamics that have a surprising dependence on the anion. Further experiments and theory will hopefully reveal more insights into the origin and nature of the lineshape dynamics in these MHC NCs by virtue of their glassy lattice response that is coupled to confined excitons.

V. CONCLUSIONS

In summary, we have applied the unique energy/time resolution of 2DE spectroscopy to model systems of MHP NCs. The 2DE signals reveal much rich dynamics, even within an inhomogeneously broadened ensemble, as promised by 2DE methods. Initially revealed is a hidden excitonic doublet, not seen in 1D spectroscopies. Relaxation from the upper to the lower excitonic state takes place

on the same 300 fs timescale as polaron formation. Polaron formation is directly observed in the homogeneous lineshape dynamics. The exciton energy trajectories are shown to correlate with the polaron formation dynamics, revealing the interaction of excitons and polarons in lead halide perovskites.

SUPPLEMENTARY MATERIAL

Additional information on materials and methods and simulations is provided in the supplementary material.

ACKNOWLEDGMENTS.

The financial support from CFI, NSERC, FQRNT, and Sony Corporation is gratefully acknowledged. PK gratefully acknowledges the enormous impact of LE Brus on not just science broadly but also his own style of doing science since he was a Ph.D. student reading the literature on quantum dots in 1994.

AUTHOR DECLARATIONS

Conflict of Interest

The authors have no conflicts to disclose.

Author Contributions

Patrick Brosseau: Conceptualization (equal); Formal analysis (equal); Investigation (equal); Methodology (equal); Software (equal). **Arnab Ghosh:** Data curation (equal); Investigation (equal). **Helene Seiler:** Conceptualization (equal); Investigation (equal); Methodology (equal); Project administration (equal); Software (equal). **Dallas Strandell:** Data curation (equal); Formal analysis (equal); Investigation (equal); Methodology (equal). **Patanjali Kambhampati:** Conceptualization (equal); Funding acquisition (equal); Investigation (equal); Project administration (equal); Supervision (equal); Writing – original draft (equal); Writing – review & editing (equal).

DATA AVAILABILITY

The data that support the findings of this study are available from the corresponding author upon reasonable request.

REFERENCES

- A. K. Jena, A. Kulkarni, and T. Miyasaka, “Halide perovskite photovoltaics: Background, status, and future prospects,” *Chem. Rev.* **119**, 3036–3103 (2019).
- H. J. Snaith, “Present status and future prospects of perovskite photovoltaics,” *Nat. Mater.* **17**, 372 (2018).
- L. Protesescu, S. Yakunin, M. I. Bodnarchuk, F. Krieg, R. Caputo, C. H. Hendon, R. X. Yang, A. Walsh, and M. V. Kovalenko, “Nanocrystals of cesium lead halide perovskites (CsPbX₃, X = Cl, Br, and I): Novel optoelectronic materials showing bright emission with wide color gamut,” *Nano Lett.* **15**, 3692 (2015).
- Q. A. Akkerman, G. Rainò, M. V. Kovalenko, and L. Manna, “Genesis, challenges and opportunities for colloidal lead halide perovskite nanocrystals,” *Nat. Mater.* **17**, 394 (2018).

- ⁵M. V. Kovalenko, L. Protesescu, and M. I. Bodnarchuk, "Properties and potential optoelectronic applications of lead halide perovskite nanocrystals," *Science* **358**, 745 (2017).
- ⁶G. Rainò, G. Nedelcu, L. Protesescu, M. I. Bodnarchuk, M. V. Kovalenko, R. F. Mahrt, and T. Stöferle, "Single cesium lead halide perovskite nanocrystals at low temperature: Fast single-photon emission, reduced blinking, and exciton fine structure," *ACS Nano* **10**, 2485 (2016).
- ⁷H. Utzat, W. Sun, A. E. K. Kaplan, F. Krieg, M. Ginterseder, B. Spokoyny, N. D. Klein, K. E. Shulenberger, C. F. Perkins, M. V. Kovalenko, and M. G. Bawendi, "Coherent single-photon emission from colloidal lead halide perovskite quantum dots," *Science* **363**, 1068 (2019).
- ⁸G. Rainò, M. A. Becker, M. I. Bodnarchuk, R. F. Mahrt, M. V. Kovalenko, and T. Stöferle, "Superfluorescence from lead halide perovskite quantum dot superlattices," *Nature* **563**, 671–675 (2018).
- ⁹H. Huang, M. I. Bodnarchuk, S. V. Kershaw, M. V. Kovalenko, and A. L. Rogach, "Lead halide perovskite nanocrystals in the research spotlight: Stability and defect tolerance," *ACS Energy Lett.* **2**, 2071 (2017).
- ¹⁰O. Yaffe, Y. S. Guo, L. Z. Tan, D. A. Egger, T. Hull, C. C. Stoumpos, F. Zheng, T. F. Heinz, L. Kronik, M. G. Kanatzidis, J. S. Owen, A. M. Rappe, M. A. Pimenta, and L. E. Brus, "Local polar fluctuations in lead halide perovskite crystals," *Phys. Rev. Lett.* **118**, 136001 (2017).
- ¹¹F. Thouin, D. A. Valverde-Chávez, C. Quarti, D. Cortecchia, I. Bargigia, D. Beljonne, A. Petrozza, C. Silva, and A. R. Srimath Kandada, "Phonon coherences reveal the polaronic character of excitons in two-dimensional lead halide perovskites," *Nat. Mater.* **18**, 349 (2019).
- ¹²L. M. Herz, "How lattice dynamics moderate the electronic properties of metal-halide perovskites," *J. Phys. Chem. Lett.* **9**, 6853 (2018).
- ¹³L. M. Herz, "Charge-carrier mobilities in metal halide perovskites: Fundamental mechanisms and limits," *ACS Energy Lett.* **2**, 1539 (2017).
- ¹⁴M. B. Johnston and L. M. Herz, "Hybrid perovskites for photovoltaics: Charge-carrier recombination, diffusion, and radiative efficiencies," *Acc. Chem. Res.* **49**, 146 (2016).
- ¹⁵A. Ghosh, D. P. Strandell, and P. Kambhampati, "A spectroscopic overview of the differences between the absorbing states and the emitting states in semiconductor perovskite nanocrystals," *Nanoscale* **15**, 2470 (2023).
- ¹⁶P. Kambhampati, "Learning about the structural dynamics of semiconductor perovskites from electron solvation dynamics," *J. Phys. Chem. C* **125**, 23571–23586 (2021).
- ¹⁷P. P. Joshi, S. F. Maehrlein, and X. Y. Zhu, "Dynamic screening and slow cooling of hot carriers in lead halide perovskites," *Adv. Mater.* **31**, 1803054 (2019).
- ¹⁸S. A. Bretschneider, I. Ivanov, H. I. Wang, K. Miyata, X. Y. Zhu, and M. Bonn, "Quantifying polaron formation and charge carrier cooling in lead-iodide perovskites," *Adv. Mater.* **30**, 1707312 (2018).
- ¹⁹K. Miyata, D. Meggiolaro, M. T. Trinh, P. P. Joshi, E. Mosconi, S. C. Jones, F. De Angelis, and X. Y. Zhu, "Large polarons in lead halide perovskites," *Sci. Adv.* **3**, e1701217 (2017).
- ²⁰K. Miyata, T. L. Atallah, and X. Y. Zhu, "Lead halide perovskites: Crystal-liquid duality, phonon glass electron crystals, and large polaron formation," *Sci. Adv.* **3**, e1701469 (2017).
- ²¹H. M. Zhu, K. Miyata, Y. P. Fu, J. Wang, P. P. Joshi, D. Niesner, K. W. Williams, S. Jin, and X. Y. Zhu, "Screening in crystalline liquids protects energetic carriers in hybrid perovskites," *Science* **353**, 1409 (2016).
- ²²F. F. Wang, Y. P. Fu, M. E. Ziffer, Y. N. Dai, S. F. Maehrlein, and X. Y. Zhu, "Solvated electrons in solids-ferroelectric large polarons in lead halide perovskites," *J. Am. Chem. Soc.* **143**, 5 (2021).
- ²³B. Guzelturk, T. Winkler, T. W. J. Van de Goor, M. D. Smith, S. A. Bourelle, S. Feldmann, M. Trigo, S. W. Teitelbaum, H.-G. Steinrück, G. A. de la Pena, R. Alonso-Mori, D. Zhu, T. Sato, H. I. Karunadasa, M. F. Toney, F. Deschler, and A. M. Lindenberg, "Visualization of dynamic polaronic strain fields in hybrid lead halide perovskites," *Nat. Mater.* **20**, 618–623 (2021).
- ²⁴X. X. Wu, L. Z. Tan, X. Z. Shen, T. Hu, K. Miyata, M. T. Trinh, R. K. Li, R. Coffee, S. Liu, D. A. Egger, I. Makasyuk, Q. Zheng, A. Fry, J. S. Robinson, M. D. Smith, B. Guzelturk, H. I. Karunadasa, X. J. Wang, X. Y. Zhu, L. Kronik, A. M. Rappe, and A. M. Lindenberg, "Light-induced picosecond rotational disordering of the inorganic sublattice in hybrid perovskites," *Sci. Adv.* **3**, e1602388 (2017).
- ²⁵Q. A. Akkerman, T. P. Nguyen, S. C. Boehme, F. Montanarella, D. N. Dirin, P. Wechsler, F. Beiglböck, G. Rainò, R. Erni, C. Katan *et al.*, "Controlling the nucleation and growth kinetics of lead halide perovskite quantum dots," *Science* **377**, 1406–1412 (2022).
- ²⁶D. Rossi, X. Liu, Y. Lee, M. Khurana, J. Puthenpurayil, K. Kim, A. V. Akimov, J. Cheon, and D. H. Son, "Intense dark exciton emission from strongly quantum confined CsPbBr₃ nanocrystals," *Nano Lett.* **20**, 7321 (2020).
- ²⁷M. A. Becker, R. Vaxenburg, G. Nedelcu, P. C. Sercel, A. Shabaev, M. J. Mehl, J. G. Michopoulos, S. G. Lambrakos, N. Bernstein, J. L. Lyons, T. Stöferle, R. F. Mahrt, M. V. Kovalenko, D. J. Norris, G. Rainò, and A. L. Efros, "Bright triplet excitons in caesium lead halide perovskites," *Nature* **553**, 189 (2018).
- ²⁸L. Hou, P. Tamarat, and B. Lounis, "Revealing the exciton fine structure in lead halide perovskite nanocrystals," *Nanomaterials* **11**, 1058 (2021).
- ²⁹P. Tamarat, M. I. Bodnarchuk, J. B. Trebbia, R. Erni, M. V. Kovalenko, J. Even, and B. Lounis, "The ground exciton state of formamidinium lead bromide perovskite nanocrystals is a singlet dark state," *Nat. Mater.* **18**, 717 (2019).
- ³⁰A. R. Srimath Kandada and C. Silva, "Exciton polarons in two-dimensional hybrid metal-halide perovskites," *J. Phys. Chem. Lett.* **11**, 3173–3184 (2020).
- ³¹F. Thouin, A. R. Srimath Kandada, D. A. Valverde-Chávez, D. Cortecchia, I. Bargigia, A. Petrozza, X. Yang, E. R. Bittner, and C. Silva, "Electron-phonon couplings inherent in polarons drive exciton dynamics in two-dimensional metal-halide perovskites," *Chem. Mater.* **31**, 7085 (2019).
- ³²Q. Sun, J. Gong, X. Yan, Y. Wu, R. Cui, W. Tian, S. Jin, and Y. Wang, "Elucidating the unique hot carrier cooling in two-dimensional inorganic halide perovskites: The role of out-of-plane carrier-phonon coupling," *Nano Lett.* **22**, 2995–3002 (2022).
- ³³Z. Nie, Z. Huang, M. Zhang, B. Wu, H. Wu, Y. Shi, K. Wu, and Y. Wang, "Hot phonon bottleneck stimulates giant optical gain in lead halide perovskite quantum dots," *ACS Photonics* **9**, 3457–3465 (2022).
- ³⁴B. Yu, L. Chen, Z. Qu, C. Zhang, Z. Qin, X. Wang, and M. Xiao, "Size-dependent hot carrier dynamics in perovskite nanocrystals revealed by two-dimensional electronic spectroscopy," *J. Phys. Chem. Lett.* **12**, 238–244 (2021).
- ³⁵M. Righetto, S. S. Lim, D. Giovanni, J. W. M. Lim, Q. Zhang, S. Ramesh, Y. K. E. Tay, and T. C. Sum, "Hot carriers perspective on the nature of traps in perovskites," *Nat. Commun.* **11**, 2712 (2020).
- ³⁶S. S. Lim, D. Giovanni, Q. Zhang, A. Solanki, N. F. Jamaludin, J. W. M. Lim, N. Mathews, S. Mhaisalkar, M. S. Pshenichnikov, and T. C. Sum, "Hot carrier extraction in CH₃NH₃PbI₃ unveiled by pump-push-probe spectroscopy," *Sci. Adv.* **5**, eaax3620 (2019).
- ³⁷M. Li, J. Fu, Q. Xu, and T. C. Sum, "Slow hot-carrier cooling in halide perovskites: Prospects for hot-carrier solar cells," *Adv. Mater.* **31**, 1802486 (2019).
- ³⁸M. J. Li, S. Bhaumik, T. W. Goh, M. S. Kumar, N. Yantara, M. Gratzel, S. Mhaisalkar, N. Mathews, and T. C. Sum, "Slow cooling and highly efficient extraction of hot carriers in colloidal perovskite nanocrystals," *Nat. Commun.* **8**, 14350 (2017).
- ³⁹Y. Yang, D. P. Ostrowski, R. M. France, K. Zhu, J. van de Lagemaat, J. M. Luther, and M. C. Beard, "Observation of a hot-phonon bottleneck in lead-iodide perovskites," *Nat. Photonics* **10**, 53 (2016).
- ⁴⁰J. H. Fu, Q. Xu, G. F. Han, B. Wu, C. H. A. Huan, M. L. Leek, and T. C. Sum, "Hot carrier cooling mechanisms in halide perovskites," *Nat. Commun.* **8**, 1300 (2017).
- ⁴¹H. Baker, C. M. Perez, C. Sonnichsen, D. Strandell, O. V. Prezhdo, and P. Kambhampati, "Breaking phonon bottlenecks through efficient auger processes in perovskite nanocrystals," *ACS Nano* **17**, 3913 (2023).
- ⁴²C. D. Sonnichsen, D. P. Strandell, P. J. Brosseau, and P. Kambhampati, "Polaronic quantum confinement in bulk CsPbBr₃ perovskite crystals revealed by state-resolved pump/probe spectroscopy," *Phys. Rev. Res.* **3**, 023147 (2021).
- ⁴³S. C. Boehme, S. ten Brinck, J. Maes, N. Yazdani, F. Zapata, K. Chen, V. Wood, J. M. Hodgkiss, Z. Hens, P. Geiregat, and I. Infante, "Phonon-mediated and weakly size-dependent electron and hole cooling in CsPbBr₃ nanocrystals revealed by atomistic simulations and ultrafast spectroscopy," *Nano Lett.* **20**, 1819 (2020).
- ⁴⁴H. Seiler, S. Palato, C. Sonnichsen, H. Baker, E. Socie, D. P. Strandell, and P. Kambhampati, "Two-dimensional electronic spectroscopy reveals liquid-like lineshape dynamics in CsPbI₃ perovskite nanocrystals," *Nat. Commun.* **10**, 4962 (2019).

- ⁴⁵P. J. Brosseau, J. J. Geuchies, D. Jasrasaria, A. J. Houtepen, E. Rabani, and P. Kambhampati, "Ultrafast hole relaxation dynamics in quantum dots revealed by two-dimensional electronic spectroscopy," *Commun. Phys.* **6**, 48 (2023).
- ⁴⁶S. Palato, H. Seiler, P. Nijjar, O. Prezhdo, and P. Kambhampati, "Atomic fluctuations in electronic materials revealed by dephasing," *Proc. Natl. Acad. Sci. U. S. A.* **117**, 11940 (2020).
- ⁴⁷H. Seiler, S. Palato, C. Sonnichsen, H. Baker, and P. Kambhampati, "Seeing multiexcitons through sample inhomogeneity: Band-edge biexciton structure in CdSe nanocrystals revealed by two-dimensional electronic spectroscopy," *Nano Lett.* **18**, 2999 (2018).
- ⁴⁸H. Seiler, S. Palato, B. E. Schmidt, and P. Kambhampati, "Simple fiber-based solution for coherent multidimensional spectroscopy in the visible regime," *Opt. Lett.* **42**, 643 (2017).
- ⁴⁹H. Seiler, B. Walsh, S. Palato, A. Thai, V. Crozatier, N. Forget, and P. Kambhampati, "Kilohertz generation of high contrast polarization states for visible femtosecond pulses via phase-locked acousto-optic pulse shapers," *J. Appl. Phys.* **118**, 103110 (2015).
- ⁵⁰H. Seiler, S. Palato, and P. Kambhampati, "Investigating exciton structure and dynamics in colloidal CdSe quantum dots with two-dimensional electronic spectroscopy," *J. Chem. Phys.* **149**, 074702 (2018).
- ⁵¹C. Sonnichsen, P. Brosseau, C. Reid, and P. Kambhampati, "OPA-driven hollow-core fiber as a tunable, broadband source for coherent multidimensional spectroscopy," *Opt. Express* **29**, 28352–28358 (2021).
- ⁵²S. Palato, H. Seiler, H. Baker, C. Sonnichsen, R. Zifkin, J. McGowan, and P. Kambhampati, "An analysis of hollow-core fiber for applications in coherent femtosecond spectroscopies," *J. Appl. Phys.* **128**, 103107 (2020).
- ⁵³D. Strandell, C. Sonnichsen, and P. Kambhampati, "Watching excitations in CsPbBr₃ perovskite nanocrystals undergo ultrafast relaxation to their emitting state," *J. Phys. Chem. C* **126**, 20505–20510 (2022).
- ⁵⁴S. Biswas, J. Kim, X. Zhang, and G. D. Scholes, "Coherent two-dimensional and broadband electronic spectroscopies," *Chem. Rev.* **122**, 4257–4321 (2022).
- ⁵⁵M. K. Petti, J. P. Lomont, M. Maj, and M. T. Zanni, "Two-dimensional spectroscopy is being used to address core scientific questions in biology and materials science," *J. Phys. Chem. B* **122**, 1771–1780 (2018).
- ⁵⁶A. Gelzinis, R. Augulis, V. Butkus, B. Robert, and L. Valkunas, "Two-dimensional spectroscopy for non-specialists," *Biochim. Biophys. Acta, Bioenerg.* **1860**, 271–285 (2019).
- ⁵⁷D. M. Jonas, "Two-dimensional femtosecond spectroscopy," *Annu. Rev. Phys. Chem.* **54**, 425–463 (2003).
- ⁵⁸M. Maiuri, M. Garavelli, and G. Cerullo, "Ultrafast spectroscopy: State of the art and open challenges," *J. Am. Chem. Soc.* **142**, 3–15 (2019).
- ⁵⁹S. Palato, H. Seiler, H. Baker, C. Sonnichsen, P. Brosseau, and P. Kambhampati, "Investigating the electronic structure of confined multiexcitons with nonlinear spectroscopies," *J. Chem. Phys.* **152**, 000021 (2020).
- ⁶⁰D. Rossi, H. Wang, Y. Dong, T. Qiao, X. Qian, and D. H. Son, "Light-induced activation of forbidden exciton transition in strongly confined perovskite quantum dots," *ACS Nano* **12**, 12436 (2018).
- ⁶¹R. R. Cooney, S. L. Sewall, E. A. Dias, D. M. Sagar, K. E. H. Anderson, and P. Kambhampati, "Unified picture of electron and hole relaxation pathways in semiconductor quantum dots," *Phys. Rev. B* **75**, 245311 (2007).
- ⁶²R. R. Cooney, S. L. Sewall, K. E. H. Anderson, E. A. Dias, and P. Kambhampati, "Breaking the phonon bottleneck for holes in semiconductor quantum dots," *Phys. Rev. Lett.* **98**, 177403 (2007).
- ⁶³S. L. Sewall, R. R. Cooney, K. E. H. Anderson, E. A. Dias, and P. Kambhampati, "State-to-state exciton dynamics in semiconductor quantum dots," *Phys. Rev. B* **74**, 235328 (2006).
- ⁶⁴P. Kambhampati, "Hot exciton relaxation dynamics in semiconductor quantum dots: Radiationless transitions on the nanoscale," *J. Phys. Chem. C* **115**, 22089 (2011).
- ⁶⁵P. Kambhampati, "Unraveling the structure and dynamics of excitons in semiconductor quantum dots," *Acc. Chem. Res.* **44**, 1 (2011).
- ⁶⁶S. L. Sewall, R. R. Cooney, K. E. H. Anderson, E. A. Dias, D. M. Sagar, and P. Kambhampati, "State-resolved studies of biexcitons and surface trapping dynamics in semiconductor quantum dots," *J. Chem. Phys.* **129**, 084701 (2008).
- ⁶⁷D. M. Sagar, R. R. Cooney, S. L. Sewall, E. A. Dias, M. M. Barsan, I. S. Butler, and P. Kambhampati, "Size dependent, state-resolved studies of exciton-phonon couplings in strongly confined semiconductor quantum dots," *Phys. Rev. B* **77**, 235321 (2008).
- ⁶⁸R. R. Cooney, S. L. Sewall, D. M. Sagar, and P. Kambhampati, "Gain control in semiconductor quantum dots via state-resolved optical pumping," *Phys. Rev. Lett.* **102**, 4127404 (2009).
- ⁶⁹R. R. Cooney, S. L. Sewall, D. M. Sagar, and P. Kambhampati, "State-resolved manipulations of optical gain in semiconductor quantum dots: Size universality, gain tailoring, and surface effects," *J. Chem. Phys.* **131**, 000013 (2009).
- ⁷⁰M. Zanni and P. Hamm, *Concepts and methods of 2D infrared spectroscopy* (2011).
- ⁷¹S. Mukamel, *Principles of Nonlinear Optical Spectroscopy* (Oxford University Press, USA, 1995).
- ⁷²Y. S. Guo, O. Yaffe, T. D. Hull, J. S. Owen, D. R. Reichman, and L. E. Brus, "Dynamic emission Stokes shift and liquid-like dielectric solvation of band edge carriers in lead-halide perovskites," *Nat. Commun.* **10**, 1175 (2019).
- ⁷³M. E. Madjet, G. R. Berdiyrov, F. El-Mellouhi, F. H. Alharbi, A. V. Akimov, and S. Kais, "Cation effect on hot carrier cooling in halide perovskite materials," *J. Phys. Chem. Lett.* **8**, 4439–4445 (2017).
- ⁷⁴B. T. Diroll, "Temperature-dependent intraband relaxation of hybrid perovskites," *J. Phys. Chem. Lett.* **10**, 5623–5628 (2019).
- ⁷⁵T. R. Hopper, A. Gorodetsky, J. M. Frost, C. Müller, R. Lovrincic, and A. A. Bakulin, "Ultrafast intraband spectroscopy of hot-carrier cooling in lead-halide perovskites," *ACS Energy Lett.* **3**, 2199–2205 (2018).
- ⁷⁶B. T. Diroll and R. D. Schaller, "Intraband cooling in all-inorganic and hybrid organic-inorganic perovskite nanocrystals," *Adv. Funct. Mater.* **29**, 1901725 (2019).
- ⁷⁷Y. Li, R. Lai, X. Luo, X. Liu, T. Ding, X. Lu, and K. Wu, "On the absence of a phonon bottleneck in strongly confined CsPbBr₃ perovskite nanocrystals," *Chem. Sci.* **10**, 5983–5989 (2019).
- ⁷⁸J. Chen, M. E. Messing, K. Zheng, and T. Pullerits, "Cation-dependent hot carrier cooling in halide perovskite nanocrystals," *J. Am. Chem. Soc.* **141**, 3532–3540 (2019).
- ⁷⁹L. Wang, Z. Chen, G. Liang, Y. Li, R. Lai, T. Ding, and K. Wu, "Observation of a phonon bottleneck in copper-doped colloidal quantum dots," *Nat. Commun.* **10**, 4532 (2019).
- ⁸⁰P. Kambhampati, "A brief discussion of chemical kinetics versus chemical dynamics," *J. Phys. Chem. Lett.* **14**, 2996–2999 (2023).